

CARBON IN SPIRAL GALAXIES FROM *HUBBLE SPACE TELESCOPE* SPECTROSCOPY¹

D. R. Garnett^{2,8}, G. A. Shields³, M. Peimbert⁴, S. Torres-Peimbert⁴, E. D. Skillman², R. J. Dufour⁵, E. Terlevich⁶, and R. J. Terlevich⁷

ABSTRACT

We present measurements of the gas-phase C/O abundance ratio in six H II regions in the spiral galaxies M101 and NGC 2403, based on ultraviolet spectroscopy using the Faint Object Spectrograph on the *Hubble Space Telescope*. The C/O ratios increase systematically with O/H in both galaxies, from $\log C/O \approx -0.8$ at $\log O/H = -4.0$ to $\log C/O \approx -0.1$ at $\log O/H = -3.4$. C/N shows no correlation with O/H. The rate of increase of C/O is somewhat uncertain because of uncertainty as to the appropriate UV reddening law, and uncertainty in the metallicity dependence on grain depletions. However, the trend of increasing C/O with O/H is clear, confirming and extending the trend in C/O indicated previously from observations of irregular galaxies. Our data indicate that the radial gradients in C/H across spiral galaxies are steeper than the gradients in O/H. Comparing the data to chemical evolution models for spiral galaxies shows that models in which the massive star yields do not vary with metallicity predict radial C/O gradients that are much flatter than the observed gradients. The most likely hypothesis at present is that stellar winds in massive stars have an important effect on the yields and thus on the evolution of carbon and oxygen abundances. C/O and N/O abundance ratios in the outer disks of spirals determined to date are very similar to those in dwarf irregular galaxies. This implies that the outer disks of spirals have average stellar population ages much younger than the inner disks.

¹Based on observations with the NASA/ESA Hubble Space Telescope obtained at Space Telescope Science Institute, which is operated by the Association of Universities for Research in Astronomy, under NASA contract NAS5-26555.

²Astronomy Department, University of Minnesota, Minneapolis MN 55455

³Astronomy Department, University of Texas, Austin, TX 78712

⁴Instituto de Astronomía, UNAM, Apdo Postal 70-264, México 04510 D.F., México

⁵Department of Space Physics and Astronomy, Rice University, Houston, TX 77251-1892

⁶Institute of Astronomy, Madingley Road, Cambridge CB3 0HA, United Kingdom

⁷Royal Greenwich Observatory, Madingley Road, Cambridge CB3 0EZ, United Kingdom

⁸Current address: Steward Observatory and Astronomy Department, University of Arizona, Tucson, AZ 85721; e-mail: garnett@oldstyle.spa.umn.edu

Subject headings: Galaxies: abundances – galaxies: evolution – galaxies: spiral – galaxies: individual: M101, NGC 2403 – galaxies: ISM – H II regions

1. Introduction

The abundance of carbon in galaxies and its evolution relative to oxygen provides fundamental information for understanding a variety of problems in stellar evolution, galaxy evolution, and the interstellar medium (ISM). A large fraction of carbon is produced in intermediate-mass stars (carbon star and planetary nebula progenitors), while oxygen is synthesized almost entirely in stars above $10 M_{\odot}$ (Maeder 1992; Woosley & Weaver 1995, hereafter WW95; Renzini & Voli 1981). The carbon abundance thus traces element enrichment over much longer timescales than oxygen, and so the C/O ratio is potentially useful as an indicator of the time since the bulk of star formation has occurred in a galaxy (e.g., Pagel & Edmunds 1978; Garnett et al. 1997a; hereafter G97a). Indeed, chemical evolution models for spiral galaxies predict very different behaviors for the evolution of C/O ratios (see discussion in Section 4 below). Additionally, cooling in dark clouds can be dominated by emission from carbon ions and carbon-bearing molecules (Tielens & Hollenbach 1985; Shull & Woods 1985), so the carbon abundance is highly relevant for the thermal balance in clouds. The variation of C/H and C/O in the ISM is important for modeling the formation of CO in molecular clouds and the possible effects of abundance variations on the I(CO)/N(H₂) relation. Evidence from the Galaxy and the Magellanic Clouds indicates that N(H)/E(B–V) varies directly with C/H (Mathis 1990), so the carbon abundance in the ISM is a potential predictor of the dust to gas ratio in galaxies.

Little data has been available for carbon abundances in the ISM of other galaxies, particularly spiral galaxies, because relatively strong emission lines from carbon in the ionized gas, particularly emission from C⁺², can be observed only in the ultraviolet spectral region. A small number of *IUE* observations of H II regions in spirals have been made (Dufour, Schiffer, & Shields 1984), but those data were often affected by low signal/noise, uncertainty in the reddening correction, and the uncertainty in matching the *IUE* emission line strengths to ground-based spectra. *HST* spectroscopy with the Faint Object Spectrograph (FOS) has improved this situation through the combination of larger dynamic range, improved detector noise characteristics, better spectral resolution, and the ability to measure both UV and optical emission lines with the same instrument and aperture (Dufour et al. 1993).

We have been carrying out a program of UV/optical spectroscopy of H II regions in a variety of galaxies with *HST* to derive reliable information on carbon abundances over a wide range of O/H. Recently completed studies of carbon abundances in metal-poor irregular galaxies have appeared in Garnett et al. (1995; hereafter G95), G97a, Kobulnicky et al. (1997), and Kobulnicky & Skillman (1998). In this paper, we present the results of FOS spectroscopy of H II regions in

the two spiral galaxies NGC 2403 and M101, from which we derived C/H and C/O abundance ratios. Sections 2 and 3 describe the observations and analysis of the spectra. Section 4 discusses the resulting abundance patterns, comparing the spiral galaxy data with our published data for irregular galaxies; we also compare the spiral galaxy data with published chemical evolution models for spiral disks, and discuss the results in the context of disk evolution and stellar nucleosynthesis.

2. Observations and Reductions

2.1. FOS Spectroscopy

We observed three H II regions in M101 and three in NGC 2403 with the FOS on *HST* during Cycle 5, using the red Digicon. For all six regions we scanned the full wavelength region from 1600 Å to 6900 Å with the four medium resolution gratings G190H, G270H, G400H, and G570H, observed through the 0".86 square (C-1) upper aperture. The beam-switch option was disabled for these observations since sky background is not a significant source of error for these observations (except for possible skyglow contamination at [O II] 2470 Å). A journal of the FOS observations is provided in Table 1.

All six H II region targets were positioned in the FOS aperture by blind offset from nearby Guide Star Catalog stars with well-measured positions. The offsets were determined from astrometry of broad-band and narrow-band H α CCD images. We attempted to maximize the signal/noise in the UV emission lines by locating regions with the highest H α emission equivalent widths in the images. However, the acquisition and slew introduces some uncertainty in the final pointing, and the resulting s/n in the UV lines varied considerably. We were able to detect both the C II] 2325 Å and C III] 1907,1909 Å emission features in four objects, while in one case we detected only C II], and in another we detected only C III].

The spectra were initially processed using the standard FOS pipeline reduction routines. Inspection of the pipeline products showed that the flat-fielding was suspect; in particular, a well-known flat field artifact at 1950 Å was prominent in absorption in the G190H spectra. In fact, the pipeline products had been processed with flats for the C-1 aperture taken in 1992 (pre-COSTAR); since that time the 1950 Å feature has disappeared. We subsequently reprocessed the spectra using flat-fields taken through the C-1 aperture in July 1996, which improved the spectra considerably.

We measured fluxes for the emission lines by direct integration of the emission line profiles, with Gaussian profile fits used for comparison and to measure blended lines. Raw measured line fluxes relative to the H β line are listed in Table 2. The 1σ uncertainties in the raw line fluxes were determined by adding in quadrature the error contributions from the following sources: the statistical noise in the lines plus local continuum, determined from the raw counts, and the uncertainty in the photometric calibration of the FOS, approximately 3% (Bohlin 1995).

Uncertainty due to gross variable features in the flat-field correction is not included. Statistical noise dominates the uncertainty in the C III] and C II] line fluxes. The upper limits listed in Table 2 represent 2σ determinations based on statistical fluctuations in the nearby continuum.

2.2. Corrections for Interstellar Reddening

Because most of the H II regions observed here are relatively metal-rich objects in spiral galaxies, and because we must compare the fluxes of UV emission lines relative to the optical spectrum, interstellar reddening and obscuration are important issues. Interstellar reddening functions toward H II complexes in other spiral galaxies are in fact not well understood. Metallicity, the intensity of star formation, the distribution of reflecting and absorbing grains, and the size of the region over which the reddening is measured may affect the shape of the obscuration curve. The UV reddening law in the Galaxy shows significant variations with line of sight (see Cardelli, Clayton, & Mathis 1989), with dense clouds associated with star formation generally showing greyer UV reddening curves. Bianchi *et al.* (1996) derived an average extinction law for stars in M31; they found an average extinction law similar to that in the Galaxy, except possibly for a weaker 2175 Å bump. Rosa & Benvenuti (1994) found a similar result based on FOS spectroscopy of OB associations in M101. The uncertainties in both of these results are still relatively large, however. Meanwhile, Calzetti, Kinney, & Storchi-Bergmann (1994) derived a mean obscuration curve for starburst regions which is quite gray relative to the Galactic obscuration curve, with a very weak or absent 2175 Å feature; furthermore, they demonstrated that the obscuration toward the stars tends to be quite different from that toward the ionized gas, a likely consequence of clumping of the interstellar gas and different spatial distributions for the OB stars and the ionized gas.

We attempted to determine the characteristics of the reddening curves for our NGC 2403 and M101 regions in several ways. We infer immediately that the reddening law is something like a Galactic law, because the FOS spectra showing strong stellar continuum also show a prominent 2175 Å bump. Therefore, we eliminate the SMC (Prévot *et al.* 1984) and Calzetti *et al.* (1994) obscuration functions from further consideration.

Cardelli *et al.* (1989) demonstrated that the obscuration function in the UV could be characterized as a smoothly varying function of R_V , the ratio of general extinction to selective extinction. Lines of sight with large R_V (≈ 5) have relatively grey UV reddening, while those with lower R_V (≈ 3) have relatively steep UV reddening curves. Most lines of sight have R_V between these two values. Therefore, we consider these two values as limits on the range of possible reddening functions for our target H II regions.

The most straightforward approach would be to compare optical/UV lines which have ratios fixed by atomic physics. He I recombination lines are a potentially very useful tool to derive the shape of the reddening curve between 2500 Å and 6700 Å. We detect He I 3187 Å and He I

2946 Å in some of our spectra, which, when combined with measurements of optical He I lines, can potentially distinguish between flat and steep UV reddening curves. Unfortunately, the signal/noise in our He I line measurements was insufficient to distinguish between $R_V = 3$ and $R_V = 5$. Improved measurements of UV He emission lines would be invaluable to constrain the reddening law in extragalactic H II regions.

A second approach is to use the slope of the UV continuum to constrain the shape of the reddening curve. Calzetti *et al.* (1994) demonstrated that the slope β (where $F_\lambda \propto \lambda^\beta$) of the UV continuum of a starburst is strongly correlated with the amount of interstellar obscuration. Starbursts that have little obscuration have UV slopes similar to theoretical predictions for young OB stellar populations ($\beta \approx -2.5$; Leitherer & Heckman 1995). Four of our six targets show stellar continuum (NGC 5461 and NGC 5471 do not); the four have continuum slopes $-2.0 < \beta < -2.25$, measured over the range 1600-2700 Å. Assuming that the star clusters are very young OB associations with little contamination from the old field star population, these slopes are consistent with modest reddening. We attempted to determine if we could distinguish between $R_V = 3.1$ and $R_V = 5$ from the dereddened slope of UV continuum. We applied $R_V = 3.1$ and $R_V = 5$ reddening functions to the spectra so that the 2175 Å feature disappeared. (This implied a higher A_V for the $R_V = 5$ case.) In all cases, the measured dereddened continuum slopes were not significantly different for the two reddening laws, and were similar to the theoretical slope. We were thus unable to constrain the reddening curves. Foreground Galactic reddening has a minor effect, contributing $A_V < 0.06$ magnitude for both galaxies, as determined from the Burstein & Heiles (1982) maps. Observations shortward of 1600 Å are likely to provide better constraints than our near-UV spectra.

Given the uncertainty in the reddening curves, we have chosen to present two sets of abundance results, based on both the $R_V = 3.1$ and $R_V = 5$ obscuration laws. The two sets of results should represent the maximum range of possible values for these spiral galaxy environments. As we shall see, the largest difference we see (for NGC 5461) is a factor of two in the derived C/O abundance ratio. While we find that the uncertainty in reddening law will not affect our conclusions regarding the general trend of C/O in spirals, we will discuss the effects on our analysis when significant.

The interstellar reddening corrections for the ionized gas were estimated from $H\alpha/H\beta$ ratios measured from the G570H spectra. In the four cases where significant stellar continuum is present, the Balmer line ratios were corrected for underlying absorption of about 1.5 Å equivalent width; this value was chosen to give the lowest dispersion in derived $A(H\beta)$ for the various line ratios. The observed line fluxes were corrected for reddening using the parameterization of Cardelli *et al.* (1989) for $R_V = 3.1$ and $R_V = 5$. The reddening-corrected line fluxes for both reddening functions are listed in Table 2; the uncertainties listed for these fluxes include an additional error term due to the uncertainty in $A(\lambda)$, as determined from the errors in the Balmer line ratios but not including the uncertainty in the shape of the reddening curve.

3. Abundance Analysis

3.1. Physical Conditions

It is necessary to have measurements of the electron density n_e and electron temperature T_e in each H II region in order to compute ion abundances directly. For our FOS spectra, it was not possible in general to make such measurements, since it was necessary to devote most of our observing time allocation to long UV exposures in order to detect the faint carbon lines. Exposure times for the optical grating settings were thus short, yielding only modest signal/noise for emission lines weaker than 10% of the $H\beta$ line. Therefore, we adopted electron temperatures and densities from published spectroscopy. The measured values for n_e and T_e are listed in Table 3. High-quality spatially resolved spectroscopy of giant H II regions (Díaz *et al.* 1987; Kinkel 1993; Kobulnicky & Skillman 1996) show that T_e varies little across such regions over size scales comparable to the FOS aperture and larger; T_e variations over small size scales can not be ruled out, however.

For the NGC 2403 objects, we generally used the temperatures and densities determined in Garnett *et al.* (1997b; G97b). However, we measured an electron density of $600\pm 200\text{ cm}^{-3}$ from the [S II] $\lambda 6717/\lambda 6731$ ratio in our FOS spectrum of VS 44, which we adopted. This results in a 9% higher O^+ abundance than for $n_e = 100\text{ cm}^{-3}$, due to the effects of collisional de-excitation on the [O II] 3727 Å doublet.

Recent spectroscopy of the M101 regions is not available, so we relied on previously published results. We found four papers (Rayo, Peimbert, & Torres-Peimbert 1982; Skillman 1985; McCall, Rybski, & Shields 1985; and Torres-Peimbert, Peimbert, & Fierro 1989) in which [O III] $\lambda 4363$ has been measured for our targets, with uncertainties quoted. A five-level atom program (De Robertis, Dufour, & Hunt 1987) was then used to derive T_e from the [O III] line measurements in these references, and the results averaged with weights determined from the errors. We did detect $\lambda 4363$ in our FOS spectrum of NGC 5471; the resulting T_e derived from this spectrum was $13300\pm 1200\text{ K}$, consistent with the published values. For the M101 regions we have no direct measurements of [O II] 7320-30 Å, so we derive T[O II] from our T[O III] values following the formulation in Garnett (1992); the resulting temperatures are listed also in Table 3. We derived electron densities from [S II] line ratios in the four references cited above; all were consistent with the low-density limit, and for the abundance analysis we adopted $n_e = 100\text{ cm}^{-3}$.

3.2. Ionic Abundances

We follow the prescriptions described in G97a,b to derive ionic abundances from the FOS spectra, using the physical conditions listed in Table 3. As in G97b, we employ a two-zone model for the temperature structure of each region to account for differences in cooling between the high- and low-ionization zones. Thus, C^{+2} , O^{+2} , Si^{+2} , and Ne^{+2} are characterized by the [O III]

electron temperature, while C^+ , N^+ , O^+ , and S^+ are characterized by T[O II].

Given the physical conditions in Table 3, we computed level populations and line emissivities $\epsilon(\lambda)$ using the five-level atom calculation. The ionic ratio then follows from

$$\frac{X^{+i}}{H^+} = \frac{\epsilon(H\beta)}{\epsilon(\lambda_i)} \frac{I(\lambda_i)}{I(H\beta)}. \quad (1)$$

The ionic abundances derived thus are listed in Table 4; two sets of abundances are shown, corresponding to the two cases of interstellar reddening we consider.

3.3. Ionization Corrections and Final Element Abundances

Since we observe both C II] and C III] as well as [O II] and [O III], we expect that any contributions to the total C and O abundances from unseen ionization states to be very small. Nevertheless, the most metal-poor, high ionization H II regions in our sample, such as NGC 5471 with $X(O^{+2}) \equiv O^{+2}/O = 0.76$, might have a non-negligible contribution from C^{+3} . Therefore, we have examined models for the photoionization of carbon in H II regions to estimate the size of such a contribution. These models are as described in G95 and G97a. In brief, the models covered the ranges 0.1-1.0 solar O/H, $35,000 \text{ K} \leq T_{eff} \leq 50,000 \text{ K}$ in stellar temperature, and $-4 \leq \log U \leq -2$ in ionization parameter.

The outcome of the modeling is displayed in Figure 1, which shows how the summed ionization fractions of C^+ and C^{+2} varies with oxygen ionization fraction $X(O^+)$. Figure 1 shows that the contribution of C^{+3} to the total carbon abundance is $< 10\%$ for a wide range of nebular ionization, and is non-negligible only for stellar temperatures $> 45,000 \text{ K}$. Only for $X(O^+) < 0.2$ can the correction for C^{+3} exceed 0.1 dex. NGC 5471, with $X(O^+) = 0.24$, has a predicted correction of at most about 10%; for the other regions, the correction to the carbon abundance is of order 5% or less. We therefore conclude that the uncertainty in the ionization correction for C^{+3} is small compared to the other sources of error for our H II region sample.

For the H II region NGC 2403-VS 38 we measured only an upper limit to the C III] line flux, and consequently only an upper limit for the C^{+2} abundance can be derived. However, we can use the derived C^+/O^+ ratio plus the derived $X(O^+)$ to estimate the C^{+2} fraction. Figure 2 shows the variation of $X(C^+)/X(O^+)$ vs $X(O^+)$ from the ionization models; note that $X(C^+)/X(O^+)$ has a small range of values at fixed $X(O^+)$. VS 38 has $X(O^+) = 0.54$; for this value $X(C^+)/X(O^+)$ is 0.8 ± 0.1 . Thus, we expect $X(C^+)$ to be 0.43 ± 0.05 . We therefore predict C^{+2}/H^+ to be 10×10^{-5} for an $R_V = 3.1$ reddening curve, or 7×10^{-5} for $R_V = 5$ reddening. Both values are consistent with the upper limits derived directly from the C III] line flux limits, and we adopt the observed $C^+/O^+ \times \text{ICF}$ for VS 38. Likewise, for NGC 5471 we have only an upper limit for C II]. For $X(O^+) = 0.24$, our models predict $C^+/C^{+2} \approx 0.27$. This is consistent with our 2σ upper limit of

0.25, given the uncertainty in the C^{+2} abundance. (At $T_e = 13,000$ K, we expect $[O\ III] \lambda 2322/H\beta \approx 0.02$, about 25-30% of our 2σ upper limit for C II]. For the other H II regions, $[O\ III] \lambda 2322$ Å emission is a negligible contribution to the measured C II] line strengths.) Thus, we are confident that our C/O ratios in all cases are representative. The total derived abundances for carbon and oxygen are listed in Table 5.

3.4. Uncertainties

The uncertainties in the final C/O abundance ratios were estimated by summing in quadrature the contributions from the line flux measurements (including uncertainty in the differential reddening), and the differential uncertainties in the C II], C III], [O II], and [O III] emissivities due to errors in T_e ; the small uncertainty in the ionization corrections for carbon is neglected.

We consider possible sources of systematic error below.

(1) *Errors in electron temperature.* A systematic error in T_e can affect the derived C^{+2}/O^{+2} and C^+/O^+ ratios, because of the large difference in excitation. C^{+2}/O^{+2} from the $\lambda 1909/\lambda 5007$ ratio varies as $e^{4.65/t}$ (where $t = T_e/10^4$ K), while C^+/O^+ from $\lambda 2325/\lambda 3727$ varies as $e^{2.34/t}$. Peimbert (1967) showed that significant fluctuations in electron temperature about the average nebular value can lead one to systematically underestimate the abundances from collisionally-excited optical/UV lines, because the forbidden line emission is weighted toward regions with higher than average T_e . If this is the case, the true C/O ratios in the H II regions could be systematically higher than our derived values. We do not expect this to affect the relative C/O values much, given the small derived values for such fluctuations in Galactic H II regions (Esteban et al. 1998), and given that there is no evidence that the postulated temperature fluctuations depend on metallicity and galaxy environment.

(2) *Depletion onto grains.* G95 discussed depletion of C and O onto grains at length. Since then, new absorption-line measurements of C and O in the local diffuse ISM have shed additional light on the subject. Meyer, Jura, & Cardelli (1998; MJC) provide additional O abundances from weak O I absorption lines, while Sofia *et al.* (1997; SCGM) have added new data on carbon abundances from weak C II] absorption lines. The sightlines in both studies were chosen to sample a wide range of physical conditions. In particular, they chose sightlines with very low fractions of molecular hydrogen; refractory elements generally show a trend of decreasing gas-phase abundance with increasing $f(H_2)$, indicating an increasing fraction of the element incorporated into dust grains. MJC and SCGM, in contrast, found that neither O nor C abundances in the local neutral gas vary with $f(H_2)$ or average gas density, but rather have very similar values toward all lines of sight that they observed. The implication from both studies is that the C and O in the diffuse gas reside in resilient grains with little exchange of C and O between gas and dust. At the same time, the dependence of element depletions on metallicity is completely unknown. A study of element

depletions for the low metallicity gas in, for example, the Magellanic Clouds is highly desirable.

The amount of C and O in grains depends on the choice of reference abundances, as discussed in Mathis (1996). Various arguments (Sofia, Cardelli, & Savage 1994; Meyer et al. 1994; Mathis 1996, MJC) suggest that the solar neighborhood B stars, with average O/H values of about 60% of the solar value (e.g., Cunha & Lambert 1994, Kilian, Montenbruck & Nissen 1994), provide a more appropriate local abundance reference for oxygen than the solar-type stars. If we adopt this argument for O and C for our H II region data, then the results of MJC and SCGM imply that our O abundances should be increased by approximately 0.1 dex and our C abundances by 0.2-0.3 dex to account for atoms locked up in grains. Esteban et al. (1998) also argue for about 0.08 dex of oxygen in grains, based on the depletion of Fe, Si, and Mg in the Orion Nebula. On the other hand, the energetic environment of giant H II regions may result in grain destruction by some unknown amount; Calzetti *et al.* (1994) noted the general absence of the 2175 Å feature in the spectra of starburst galaxies, and have argued that this may be the result of grain destruction. On the other hand, we clearly see the 2175 Å feature in our spectra, so grain destruction remains an open question. For this paper, we choose not to apply a correction for grains to our derived abundances, but the reader should keep in mind that the actual C/O ratios may be higher by 0.1-0.2 dex for both the spiral and the dwarf galaxy data.

4. Discussion

4.1. The Variation of C, N, and O in NGC 2403 and M101

Figure 3 displays the derived C/O ratios for the NGC 2403 and M101 H II regions as a function of O/H. The open symbols in this figure show C/O for an $R_V = 3.1$ reddening law; filled symbols show the $R_V = 5$ case. Despite the uncertainty in the reddening law, the data clearly show that C/O increases with O/H in the two spiral galaxies. The actual rate of increase can not be determined precisely without better knowledge of the reddening corrections and depletion factors, although the observed trend in C/O is at least as steep as the one derived by G95. When the Orion Nebula and solar abundances are included, there is some indication that C/O levels off at higher metallicities.

Our new results show clearly an increase in C/O with O/H as had been noted by G95 from observations of H II regions in irregular galaxies. This is demonstrated graphically in Figure 4, where we plot the spiral galaxy data together with published data for irregular galaxies. The spiral galaxy points merge smoothly with and extend the trend over the range $-4.0 < \log \text{O/H} < -3.3$. At present it is not possible to tell if the trend in C/O flattens at lower O/H (in which case I Zw 18 could be considered to have normal C/O), or if C/O continues to decline at lower O/H (in which case I Zw 18 would have unusually high C/O). Additional data on C/O in metal-poor irregular galaxies are needed to clearly show if C/O flattens at the highest and/or lowest metallicities.

G95 also noted an apparent trend of increasing C/N with O/H in the irregulars, with an abrupt decline in C/N for the Orion nebula and solar neighborhood stars, and suggested that the trend could reflect the differences in star formation histories between spirals and irregulars. Our new spiral galaxy data suggest a considerably different picture, as shown in Figure 5. With our new data added, no significant trend is seen in C/N vs. O/H, either in the combined data, or in the spiral galaxy data considered separately. Even if we exclude the low points for NGC 5253, which may be contaminated by N-enriched Wolf-Rayet star ejecta (Kobulnicky et al. 1997), no correlation is evident. It may be, therefore, that the trend in C/N noted by G95 was the result of a limited number of data points. The absence of a trend in C/N indicates that the two elements are injected into the ISM on similar timescales.

4.2. Evolution of C/O vs. O/H: Solar Neighborhood Models

The interpretation of the trend of carbon abundances involves an extra level of complexity, because carbon can be synthesized in long-lived intermediate mass stars as well as massive stars. Tinsley (1979) showed that a primary element, such as C, that is produced in long-lived stars can mimic the behavior of a secondary element, because of the delay in ejection of C into the ISM. As a result, the instantaneous recycling approximation can not be applied for carbon. Thus, one must either model the evolution numerically, or model the delayed ejection with an analytic approximation as in Pagel (1989).

In G95, we compared the observed trend for C/O with O/H in irregular galaxies with the results of chemical evolution computations for the evolution of C/O in the solar neighborhood. On the basis of those models, we concluded that the observed variation in C/O was best explained with the metallicity-dependent yields for carbon and oxygen derived for massive stars with radiatively-driven mass loss (Maeder 1992), plus the intermediate mass star contribution. Models which used hydrostatic massive star model yields failed to predict a steep enough increase in C/O at high O/H. Here we re-examine the comparison of models with our new results.

Figure 6 shows C/O vs. O/H for the combined spiral and irregular galaxy sample, along with a few representative models for the evolution of C/O in the solar neighborhood. Figure 6(a) shows models by Carigi (1994, 1996), using massive star yields from Maeder (1992), which include the effects of mass loss on C and O yields; Figure 6(b) shows the predictions of models by Timmes, Woosley, & Weaver (1995) and Chiappini, Matteucci, & Gratton (1997); both use the massive star yields of Woosley & Weaver (1995), which do not include the effects of stellar mass loss. All of the models shown use Renzini & Voli (1981) as the source for intermediate mass star yields for carbon and other elements.

The effect of the choice of massive star yields is clear comparing Fig. 6(a) with Fig. 6(b): the models with Maeder yields show steeper increases in C/O at high metallicities. (The models of Prantzos, Vangioni-Flam, & Chauveau 1994 show similar behavior.) Do the data favor one family

of models? Unfortunately, the answer depends on the assumed UV reddening function. When the flatter UV reddening is used, the data are consistent with the models using WW95 yields. On the other hand, with the steeper $R_V = 3$ reddening function the data are more consistent with the models using Maeder’s massive star yields. Improved UV spectra to determine the proper reddening correction for metal-rich H II regions are needed to distinguish clearly between the two families of chemical evolution models.

At the same time, solar neighborhood chemical evolution models may not provide a unique representation of the evolution of C/O vs. O/H. For example, compare the Carigi (1996) model in Fig. 6(a) with the Carigi (1994) model. Both use the same yields, yet the abundance evolution is noticeably different. One explanation for the differences is that Carigi (1996) uses a star formation law with a steeper dependence on gas surface density than Carigi (1994). As a result, in the Carigi (1996) model star formation and enrichment progress more slowly; because of the slower evolution, carbon production from lower mass stars has a chance to “catch up” more quickly with the oxygen production, and so C/O is higher in the 1996 models at low O/H. This may also account for the difference between the Timmes et al. and Chiappini et al. models, since Timmes et al. use a steeper star formation law than Chiappini et al. One can infer from this exercise that the evolution of C/O with O/H is sensitive to the star formation/enrichment timescale. Therefore, solar neighborhood models are not likely to predict correctly the evolution of abundance ratios in regions with different gas consumption timescales.

What about the abundances as a function of the gas mass fraction μ_g ? Figure 7 shows the abundance ratios O/H and C/O as a function of $\ln \mu_g$. Gas fractions for NGC 2403 were taken from G97b. For M101, we used H I measurements from Kamphuis (1993), CO measurements from Kenney, Scoville, & Wilson (1991), and surface photometry from Okamura, Kanazawa, & Kodaira (1976) to construct the gas fraction profile, assuming that NGC 2403 and M101 have the same stellar mass/light ratio; we also assumed for convenience a symmetric gas profile for M101, although the observations of Kamphuis show that the H I surface density is not symmetric about the galaxy’s minor axis. We do not use dynamical models to determine masses because of the uncertain effect of dark matter on the comparison between models and observations. Although it is difficult to estimate uncertainties precisely for H₂ column densities derived from CO measurements and for disk M/L ratios, we assign a provisional uncertainty of $\pm 20\%$ for the derived gas fractions.

Figure 7 shows predictions of abundances vs. gas fraction for the models of Carigi (1996) and Chiappini et al. (1997). The Carigi model (*solid curve*) again shows a steep increase in C/O due to the effects of stellar mass loss on the massive star yields. This model provides a good qualitative match to the trend of the M101 data points, although it systematically overpredicts both C/O and O/H. The discrepancy is somewhat reduced if a modest amount (0.1-0.2 dex) of C and O in the ionized gas is in dust grains. On the other hand, the Chiappini et al. model (*dashed curve*) shows very flat behavior for C/O once the gas fraction falls below 50% ($\ln \mu \approx -0.6$). This model would be qualitatively consistent with the observations for the case of the $R_V = 5$ reddening function, it would fail to explain the steeply rising C/O if the $R_V = 3$ reddening function applies.

The comparison here highlights again the need for additional, improved measurements of UV reddening and emission line strengths.

We see marginal evidence for systematically higher C/O at a given μ in M101 than in NGC 2403. This may be related to the observation that interstellar abundances are higher overall in more massive spirals (G97b). However, with the limited amount of available data nothing definite can be concluded at this time about differences in C/O ratios between spirals.

4.3. Radial Gradients in C/O and Chemical Evolution Models

Another key test of the chemical evolution models is whether they reproduce the spatial distribution of heavy elements across the galaxies. Radial gradients in the oxygen abundance are commonly observed in spirals, and the various published chemical evolution models generally reproduce the O/H gradients. Now we have information on the spatial distribution of carbon in two galaxies, which potentially provides additional constraints on the models. The questions are whether we see gradients in C/O in these galaxies, and whether existing chemical evolution models reproduce the observed trends.

Before we can discuss these questions, it is necessary to determine how best to compare the models with the data for NGC 2403 and M101. Few theoretical studies have discussed the spatial distribution of carbon in spirals, presumably because of a lack of measurements to compare with the models. The three studies which do provide spatial distributions for carbon (Carigi 1996, Götz & Köppen 1992, and Mollá et al. 1997) present results based on models for the Galaxy. Mollá et al. presented models for a few other spirals (not for NGC 2403 or M101, however), but the variation in their predicted C/O gradients is small. Direct comparison of model abundance gradients, in dex/kpc, for the Milky Way with observations of other spirals is not informative, because spirals come in a variety of sizes. However, G97b showed that high surface brightness spiral galaxies have similar oxygen abundance gradients when plotted per unit scale length, with no correlation with galaxy luminosity. This offers a potential way to scale the Milky Way models for comparison with other galaxies, and we do so here. For the purposes of our discussion, we adopt the following disk scale lengths: $R(\text{scale}) = 2.1$ kpc for NGC 2403 (based on the photometry of Okamura, Takase, & Kodaira 1977, plus the Cepheid distance of Tammann & Sandage 1968); $R(\text{scale}) = 3.5$ kpc for the Galaxy (de Vaucouleurs & Pence 1978); and 5.4 kpc for M101 (Okamura et al. 1976, plus the Cepheid distance of Kelson et al. 1996). We then normalize galactocentric distances in the observational sample and in the chemical evolution models by $R(\text{scale})$.

We plot the abundance data for NGC 2403 and M101 as a function of the normalized radius $R/R(\text{scale})$ in Figures 8 and 9, with the Milky Way chemical evolution models overplotted. Note first of all that the observations imply that both NGC 2403 and M101 show significant radial gradients in C/O, of order -0.1 to -0.2 dex/scalelength.

The upper panels of Figs. 8 and 9 show that all of the chemical evolution models considered

here do an adequate job of reproducing the slope of the abundance gradients, when normalized to the disk scalelength. The models tend to predict significantly higher O abundances at a given R/R(scale) than observed in NGC 2403. This may reflect a real difference in the global enrichment. G97b noted that the most luminous spirals have higher abundances at a fixed value of disk surface brightness than their less luminous counterparts. This reflects the relationship between galaxy mass and metallicity observed in spiral galaxies (Garnett & Shields 1987, Zaritsky, Kennicutt, & Huchra 1994).

The lower panels in Figs. 8-9 compare the model calculations for the radial variation of C/O with our data. In contrast to the case of O/H, the models vary widely in their predictions for the variation of C/O. The model of Carigi (1996) in Figure 8 appear to be an adequate match for the M101 data, although the model somewhat overpredicts both C/O and O/H. This discrepancy is reduced if a modest amount of C and O are in dust grains. Alternatively, the derived O/H could be too low because of temperature fluctuations (Peimbert 1995), or perhaps the formation of black holes by massive stars above a certain mass reduces the stellar yields (Maeder 1992). The systematically lower abundances in NGC 2403 await an explanation; this may be related to the question of what mechanism is responsible for the mass-metallicity relation for galaxies. On the other hand, the models of Götz & Köppen (1992) and Mollá et al. (1997), shown in Fig. 9, produce C/O gradients which are too shallow compared to the data. Götz & Köppen, in fact, predict a slight *increase* in C/O progressing outward. Mollá et al. actually predict a range in C/O gradients for the galaxies they modeled, 0.0 to -0.01 dex/kpc; here we used their steepest predicted gradient, computed for the Milky Way.

Curiously, the models in Figure 9 do not fail by producing too little C in the inner disks, as one might have expected since both models use Santa Cruz massive star yields computed with without stellar mass loss. Instead, both models predict too much carbon in the outer disks. Note, however, that Götz & Köppen artificially increased the yield of carbon in their model by a factor of three, motivated by the failure of their model to reproduce the solar carbon abundance. A uniform reduction in their C abundances by a factor three would bring their outer disk abundances in line with our observed C/O in NGC 5471, and then they would underproduce C in the inner disks, as expected. On the other hand, the implied high C/O in the outer disks of the Mollá et al. models is more difficult to understand. It seems clear that explaining the heavy element abundance pattern in the outer disks of spiral galaxies remains a challenge to theoretical models.

5. Conclusions

Because of the unique ultraviolet spectroscopic capability of the *Hubble Space Telescope*, we are able to present the first significant sampling of the spatial distribution of carbon abundances in spiral galaxies. We have shown that there are radial gradients in C/O across the disks of both NGC 2403 and M101, in the sense that the C/H gradients are steeper than the gradients in O/H. On the other hand, our ability to determine the actual magnitude of the C/O gradients is limited

because of the uncertainty in the choice of UV reddening function. C/N appears to show no correlation with O/H, as might be expected if both are produced in similar stellar mass ranges. Again, however, more and improved data are needed to reduce some of the scatter seen in Figure 5, to more precisely constrain systematic trends in C/N.

The next observational step will be to obtain improved UV spectroscopy with sufficient signal/noise in the UV He I lines to constrain the reddening, as well as improved signal/noise in the C III] and C II] lines themselves, and to possibly detect N III] 1750 Å. (The best approach would be to observe O III] 1661-6 Å together with C III], which would minimize the uncertainties due to errors in reddening and temperature; however, such observations may not be possible with existing HST spectrographs.) In addition, it is well established that abundance gradient determinations based on only a few data points can be very inaccurate (Zaritsky, Kennicutt, & Huchra 1994), and spiral galaxies may show asymmetries in the abundance distribution (e.g., M101: Kennicutt & Garnett 1996). It will be necessary, therefore, to obtain observations of additional regions to accurately define the radial distribution of carbon in these galaxies.

At the same time, it is clear that additional theoretical work is needed to understand the evolution of carbon in galaxies. Few theoretical studies so far have addressed the evolution of carbon, yet carbon is an important diagnostic of both stellar yields and the enrichment timescales. One important aspect to understand is the problem of the abundance pattern in outer spiral disks. The CNO abundance ratios in outer disks are very similar to those observed in dwarf irregular galaxies (see also Ferguson et al. 1998, van Zee et al. 1998). This might be difficult to understand in the context of a disk which is more or less uniformly old, but has had the outer disk abundances modified by slow accretion of metal-poor gas from the outer galaxy. The implication is that outer spiral disks have experienced slow star formation much like the dwarf irregular galaxies, and that the average age of stars in outer spiral disks is much smaller than in the inner disk (cf. Allen, Carigi, & Peimbert 1998). This is consistent with the concept of “inside-out” build-up of the disk, in which the timescale for accretion of gas onto the forming disk increases radially outward (e.g., Chiappini et al. 1997).

One important question is whether the similarity of outer spiral disk abundances to the irregular galaxies is a general phenomenon, or whether there are significant differences between late-type spirals and early-type spirals. We have obtained only a small number of data points in two Sc-type spirals, barely the tip of an iceberg. Additional, improved measurements of abundances of carbon and nitrogen will provide new and interesting information on similarities and differences in the evolution of spiral disks.

We thank Denise Taylor and Tony Keyes at STScI for their very helpful assistance in implementing this program; Tony also kindly provided the updated FOS flat fields upon request. We also thank Rene Walterbos for providing ground-based images for some of our targets, and Michael Rosa for supplying coordinates for his earlier FOS observations of the M101 H II regions. DRG and MP thank Leticia Carigi and Cristina Chiappini for extensive and informative

discussions of the chemical evolution models and for providing tables of numerical results. Support for this program was provided by NASA and STScI through grant GO-6044-94A. DRG also acknowledges support from NASA-LTSARP grant NAG5-6416, while EDS acknowledges support from NASA-LTSARP grant NAGW-3189.

REFERENCES

- Allen, C., Carigi, L., & Peimbert, M., 1998, *ApJ*, 494, 247
- Bianchi, L., Clayton, G. C., Bohlin, R. C., Hutchings, J. B., & Massey, P., 1996, *ApJ*, 471, 203
- Bohlin, R. C., 1995, in *Calibrating Hubble Space Telescope: Post Servicing Mission* eds. A. Koratkar and C. Leitherer (Baltimore: STScI), p. 49
- Burstein, D., & Heiles, C. 1982, *AJ*, 87, 1165
- Calzetti, D., Kinney, A. L., & Storchi-Bergmann, T., 1994, *ApJ*, 429, 582
- Cardelli, J. A., Clayton, G. C., & Mathis, J. S., 1989, *ApJ*, 345, 245
- Carigi, L., 1994, *ApJ*, 424, 181
- Carigi, L., 1996, *Rev. Mexicana Astron. Astrofis.*, 32, 179
- Chiappini, C., Matteucci, F., & Gratton, R., 1997, *ApJ*, 477, 765
- Cunha, K., & Lambert, D. L. 1994, *ApJ*, 426, 170
- De Robertis, M. M., Dufour, R. J., & Hunt, R. W., 1987, *JRASC*, 81, 195
- de Vaucouleurs, G., & Pence, W. D., 1978, *AJ*, 83, 1163
- Díaz, A. I., Terlevich, E., Pagel, B. E. J., Vilchez, J. M., & Edmunds, M. G., 1987, *MNRAS*, 226, 19
- Dufour, R. J., Schiffer, F. H., & Shields, G. A. 1984, in *Future of Ultraviolet Astronomy Based on Six Years of IUE Research*, eds. J. Mead, R. Chapman, & Y. Kondo, (Washington, D.C.: NASA) NASA CP-2349, p. 111
- Dufour, R. J., Skillman, E. D., Garnett, D. R., Shields, G. A., Peimbert, M., Torres-Peimbert, S., Terlevich, E., & Terlevich, R., 1993, *Rev. Mexicana Astron. Astrofis.*, 27, 115
- Esteban, C., Peimbert, M., Torres-Peimbert, S., & Escalante, V., 1998, *MNRAS*, 295, 401
- Ferguson, A. M. N., Gallagher, J. S., & Wyse, R. F. G. 1998, *AJ*, in press
- Garnett, D. R., 1992, *AJ*, 103, 1330
- Garnett, D. R., & Shields, G. A., 1987, *ApJ*, 317, 82
- Garnett, D. R., Skillman, E. D., Dufour, R. J., Peimbert, M., Torres-Peimbert, S., Terlevich, R., Terlevich, E., & Shields, G. A., 1995, *ApJ*, 443, 64 (G95)
- Garnett, D. R., Skillman, E. D., Dufour, R. J., & Shields, G. A. 1997a, *ApJ*, 481, 174 (G97a)
- Garnett, D. R., Shields, G. A., Skillman, E. D., Sagan, S. P., & Dufour, R. J. 1997b, *ApJ*, 489, 63 (G97b)
- Götz, M., & Köppen, J., 1992, *A&A*, 260, 455
- Kamphuis, J., 1993, PhD thesis, University of Groningen
- Kelson, D. D., et al., 1996, *ApJ*, 463, 26

- Kenney, J. D. P., Scoville, N. Z., & Wilson, C. D., 1991, *ApJ*, 366, 432
- Kennicutt, R. C. Jr., & Garnett, D. R., 1996, *ApJ*, 456, 504
- Kilian, J., Montenbruck, O., & Nissen, P. E., 1994, *A&A*, 284, 437
- Kinkel, U., 1993, PhD thesis, University of Heidelberg
- Kobulnicky, H. A., & Skillman, E. D., 1996, *ApJ*, 471, 211
- Kobulnicky, H. A., & Skillman, E. D., 1998, *ApJ*, 497, 601
- Kobulnicky, H. A., Skillman, E. D., Roy, J.-R., Walsh, J., & Rosa, M., 1997, *ApJ*, 477, 679
- Leitherer, C., & Heckman, T. M., 1995, *ApJS*, 96, 9
- Maeder, A., 1992, *A&A*, 264, 105
- Mathis, J. S. 1990, *ARAA*, 28, 37
- Mathis, J. S. 1996, *ApJ*, 472, 643
- Matteucci, F., & François, P., 1989, *MNRAS*, 239, 885
- McCall, M. L., Rybski, P. M., & Shields, G. A., 1985, *ApJS*, 57, 1
- Meyer, D. M., Jura, M., Hawkins, I., & Cardelli, J. A., 1994, *ApJ*, 437, L59
- Meyer, D. M., Jura, M., & Cardelli, J. A., 1998, *ApJ*, 493, 222 (MJC)
- Mollá, M., Ferrini, F., & Díaz, A. I., 1997, *ApJ*, 475, 519
- Okamura, S., Kanazawa, T., & Kodaira, K., 1976, *PASJ*, 28, 329
- Okamura, S., Takase, B., & Kodaira, K., 1977, *PASJ*, 29, 567
- Pagel, B. E. J., 1989, *Rev. Mexicana Astron. Astrofis.*, 18, 153
- Pagel, B. E. J., & Edmunds, M. G., 1978, *MNRAS*, 185, 77P
- Peimbert, M. 1967, *ApJ*, 150, 825
- Peimbert, M. 1995, in *The Analysis of Emission Lines*, eds. R. E. Williams and M. Livio, (Cambridge: Cambridge University Press), 165
- Prantzos, N., Vangioni-Flam, E., & Chauveau, S., 1994, *A&A*, 285, 132
- Prévot, M. L., Lequeux, J., Maurice, E., Prévot, L., & Rocca-Volmerange, E., 1984, *A&A*, 132, 389
- Rayo, J. F., Peimbert, M., & Torres-Peimbert, S., 1982, *ApJ*, 255, 1
- Renzini, A., & Voli, M., 1981, *A&A*, 94, 175
- Rosa, M. R., & Benvenuti, P., 1994, *A&A*, 291, 1
- Shull, J. M., & Woods, D. T. 1985, *ApJ*, 288, 50
- Sofia, U. J., Cardelli, J. A., Guerin, K. P., & Meyer, D. M., 1997, *ApJ*, 482, L105 (SCGM)
- Sofia, U. J., Cardelli, J. A., & Savage, B. D., 1994, *ApJ*, 430, 650

- Skillman, E. D., 1985, *ApJ*, 290, 449
- Tammann, G. A., & Sandage, A., 1968, *ApJ*, 151, 825
- Tielens, A. G. G. M., & Hollenbach, D. J., 1985, *ApJ*, 291, 722
- Timmes, F. X., Woosley, S. E., & Weaver, T. A., 1995, *ApJS*, 98, 617
- Tinsley, B. M., 1979, *ApJ*, 229, 1046
- Torres-Peimbert, S., Peimbert, M., & Fierro, J., 1989, *ApJ*, 345, 186
- Walter, D. K., Dufour, R. J., & Hester, J. J., 1992, *ApJ*, 397, 196
- Woosley, S. E., & Weaver, T. A., 1995, *ApJS*, 101, 181
- van Zee, L., Salzer, J. J., Haynes, M. P., O'Donoghue, A. A., & Balonek, T. J., 1998, *AJ*, in press.
- Zaritsky, D., Kennicutt, R. C., Jr., & Huchra, J. P., 1994, *ApJ*, 420, 87

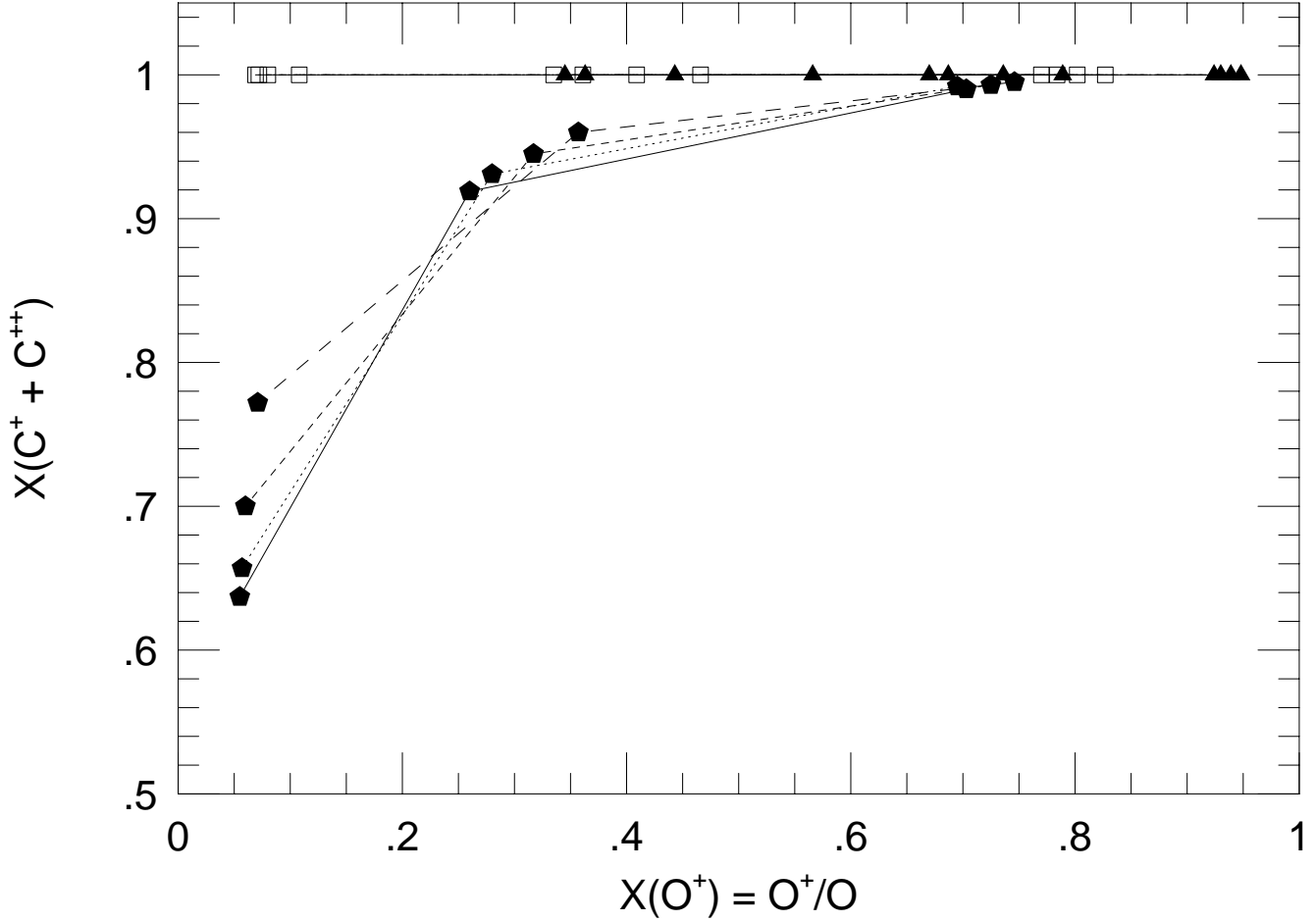


Fig. 1.— Photoionization model calculations for the ionization of carbon and oxygen in H II regions. The plot shows the volume fraction of C in C^+ and C^{++} versus the volume fraction of O in O^+ . Filled triangles represent models with $T_{eff} = 35,000$ K, open squares $T_{eff} = 40,000$ K, and filled pentagons $T_{eff} = 50,000$ K. Solid line: represents models with 0.2 times solar heavy element abundances; dotted line = 0.5 times solar abundances; short-dashed line = solar abundances; long-dashed line = 2 times solar abundances. The ionization parameter decreases from right to left in the plot, from $\log U = -2$ to $\log U = -4$. All of the objects in our study have $X(O^+) > 0.2$, implying negligible corrections for unobserved C^{+3} .

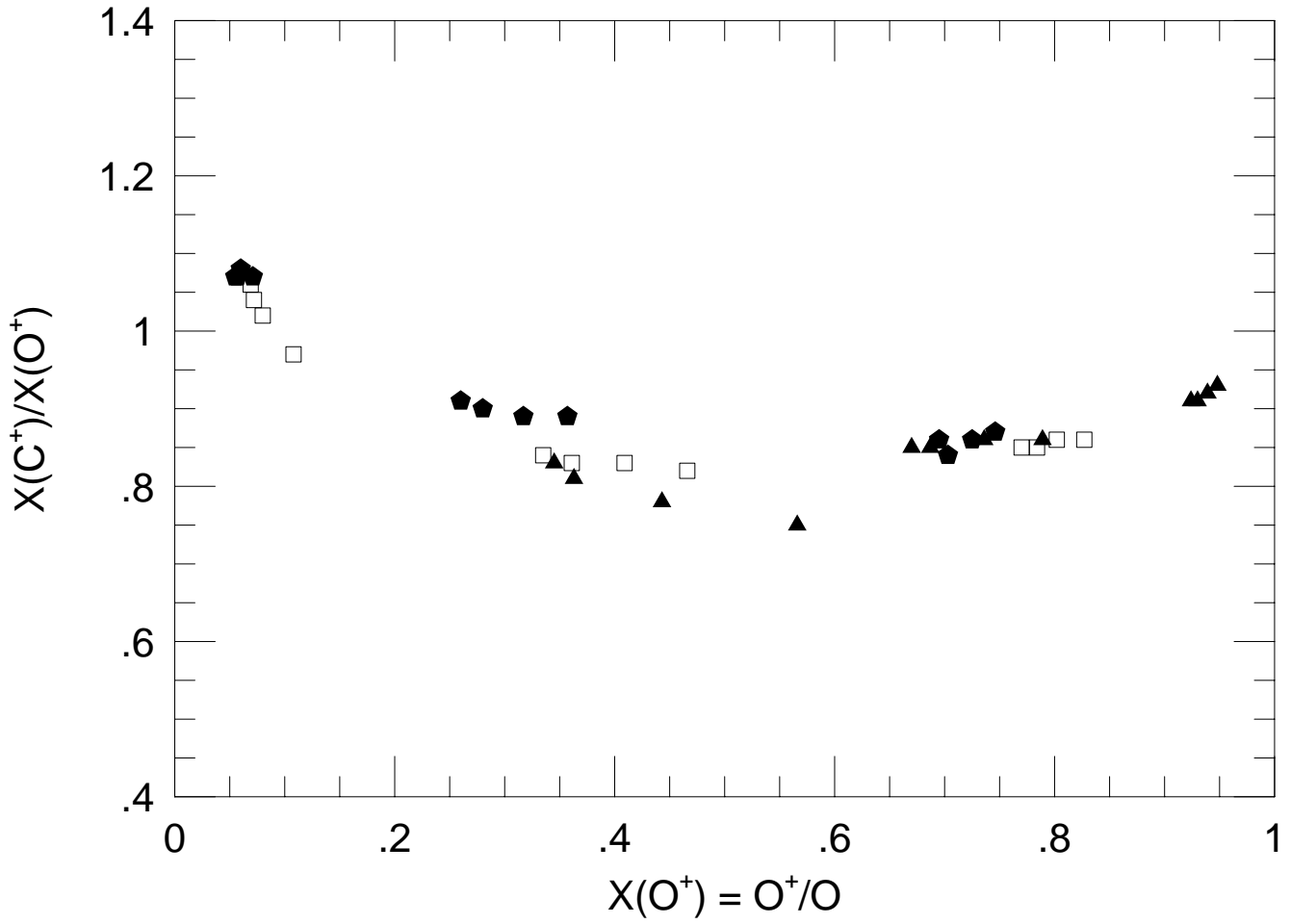


Fig. 2.— Similar to Figure 1, showing $X(C^+)/X(O^+)$ vs. $X(O^+)$, based on the photoionization models.

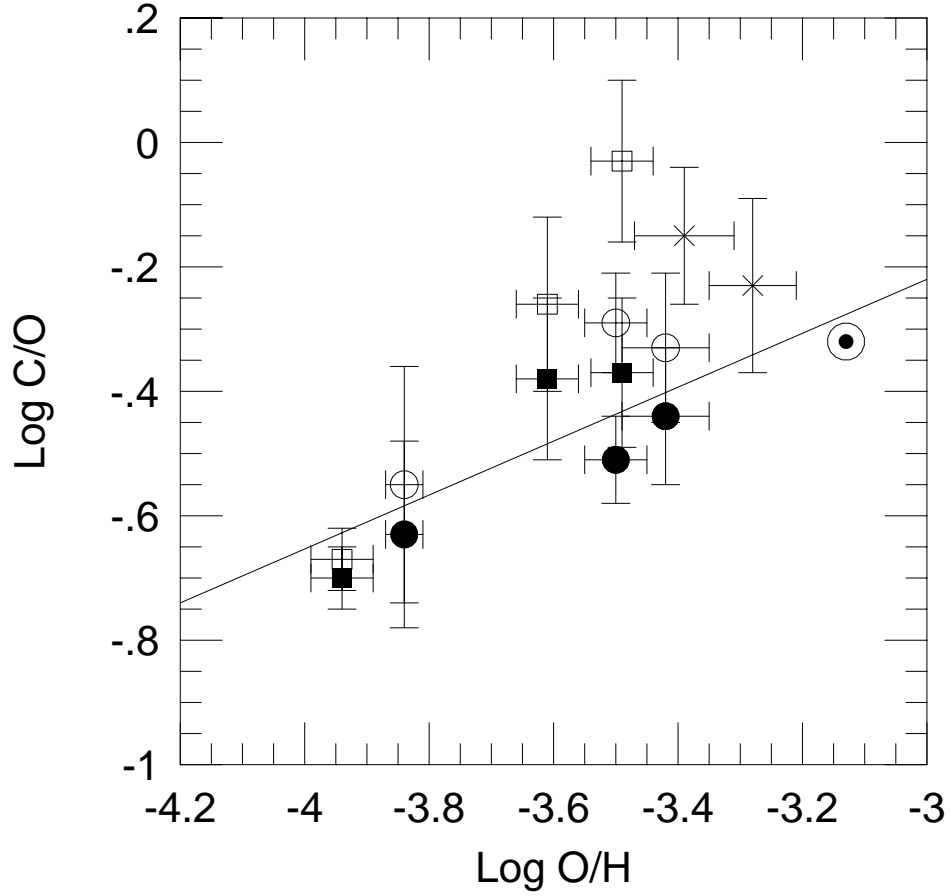


Fig. 3.— Log C/O vs. log O/H for the NGC 2403 (circles) and M101 (squares) H II regions. The open symbols represent the abundances derived using a reddening function with $R_V = 3.1$ to correct the spectra; filled symbols show the values based on an $R_V = 5$ reddening function. Crosses are the values for the Orion Nebula from Walter et al. (1992) and Esteban et al. (1998). The line represents the relation derived by G95 for irregular galaxies.

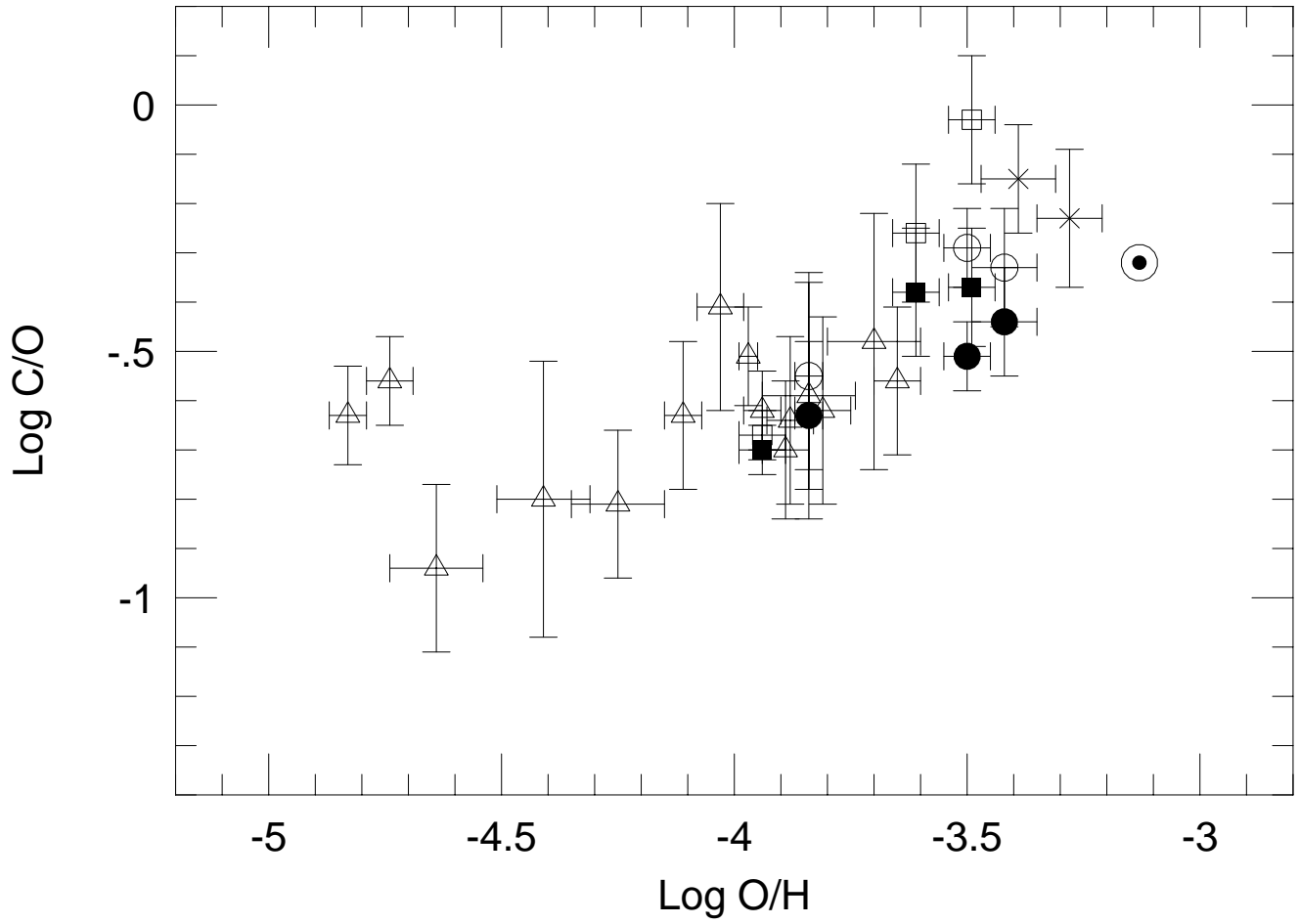


Fig. 4.— Same as in Figure 3, but with abundance data for dwarf irregular galaxies and the Magellanic Clouds plotted as triangles (Garnett et al. 1995, 1997a, Kobulnicky & Skillman 1998).

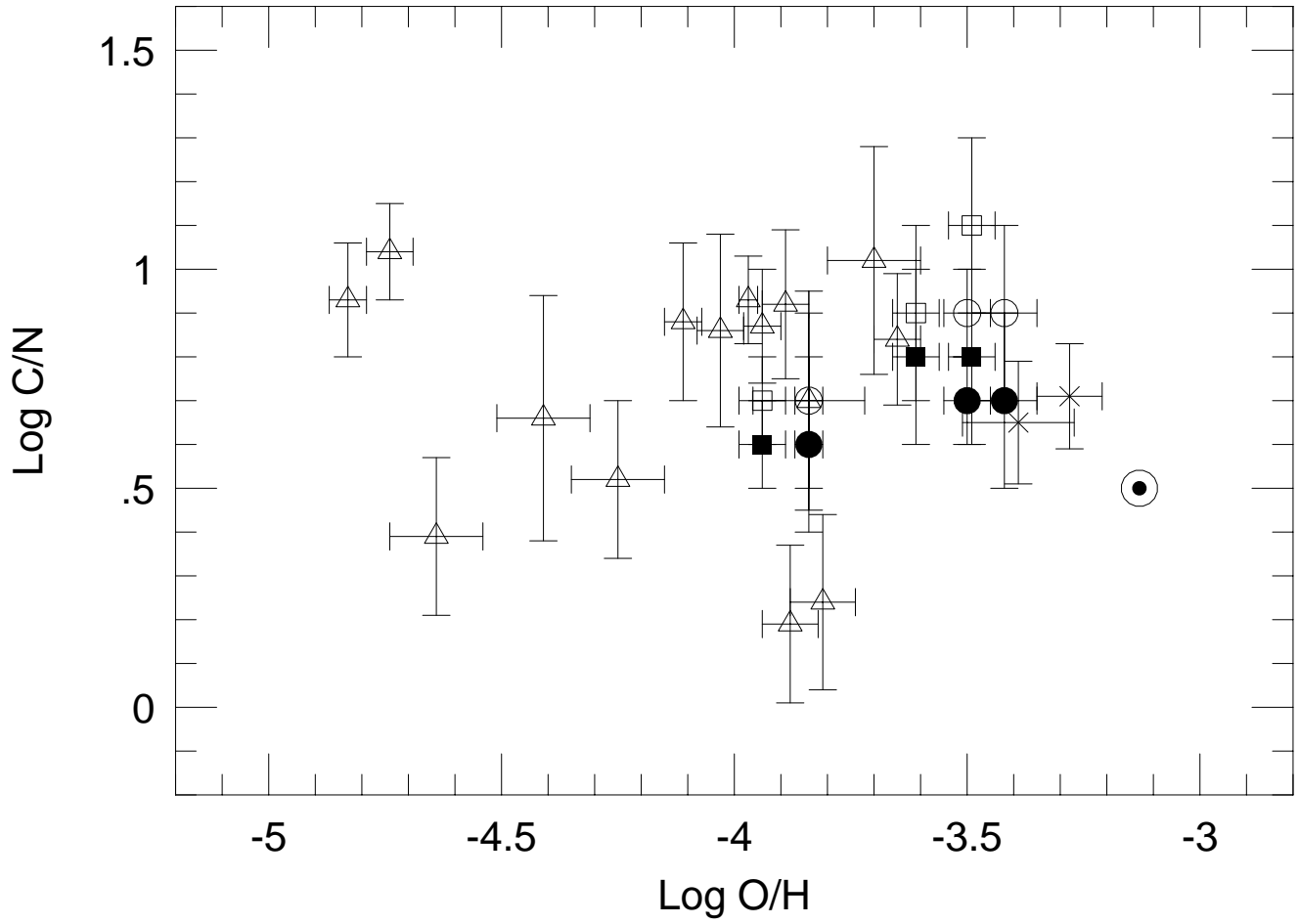


Fig. 5.— C/N vs. O/H for the H II regions shown in Figure 4. The two lowest points near $\log O/H = -3.85$ are the N-rich regions of NGC 5253 (Kobulnicky et al. 1997).

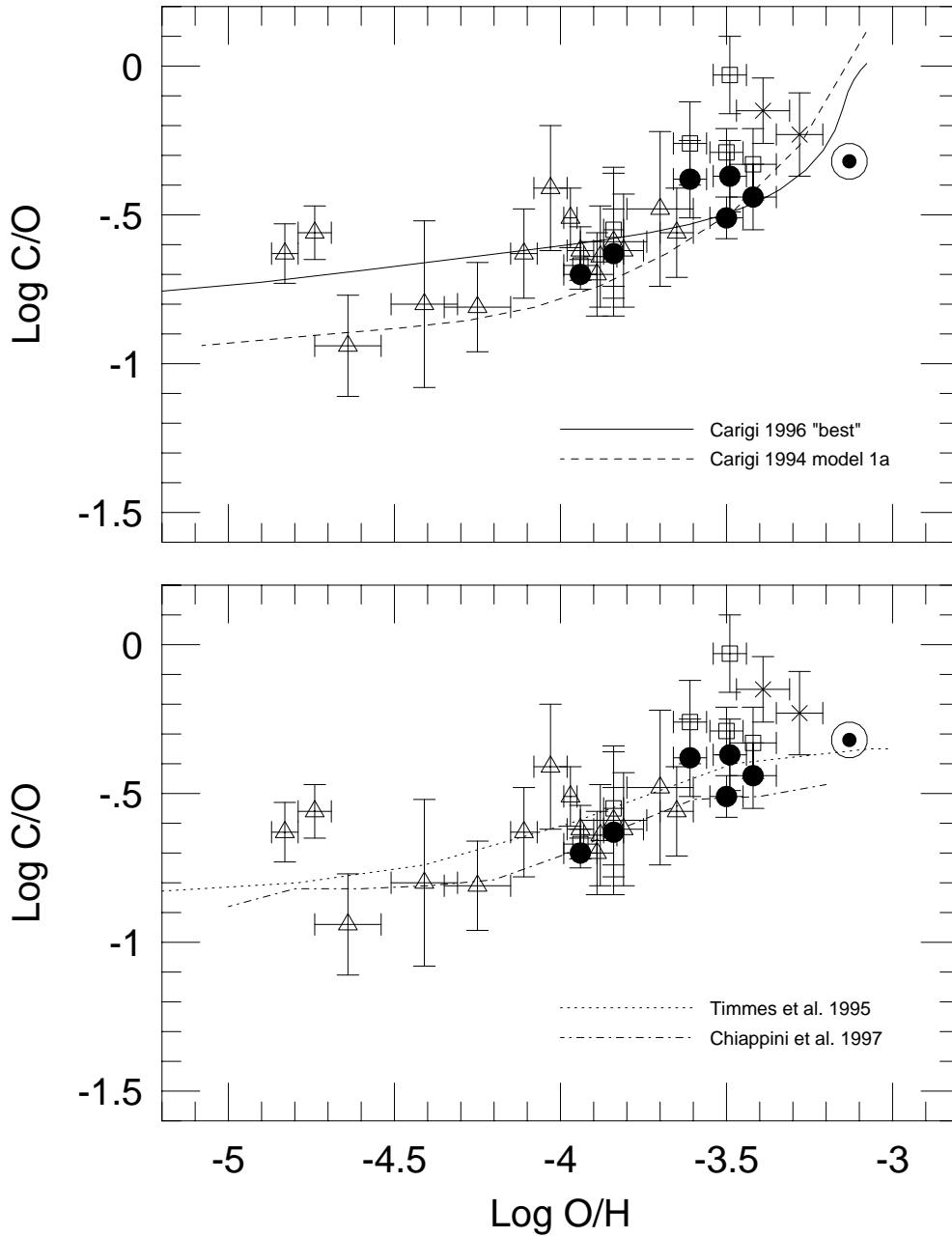


Fig. 6.— Carbon abundance data for spiral and irregular galaxies compared with models for the evolution of C/O in the solar neighborhood. (a) Solid line: the “best model” of Carigi (1996); dashed line: model 1a from Carigi (1994). These models employ the metallicity-dependent yields from Maeder (1992) for massive stars. (b) Chemical evolution models using massive star yields from Woosley & Weaver (1995). Dotted line: Timmes et al. (1995); dot-dash line: Chiappini et al. (1997).

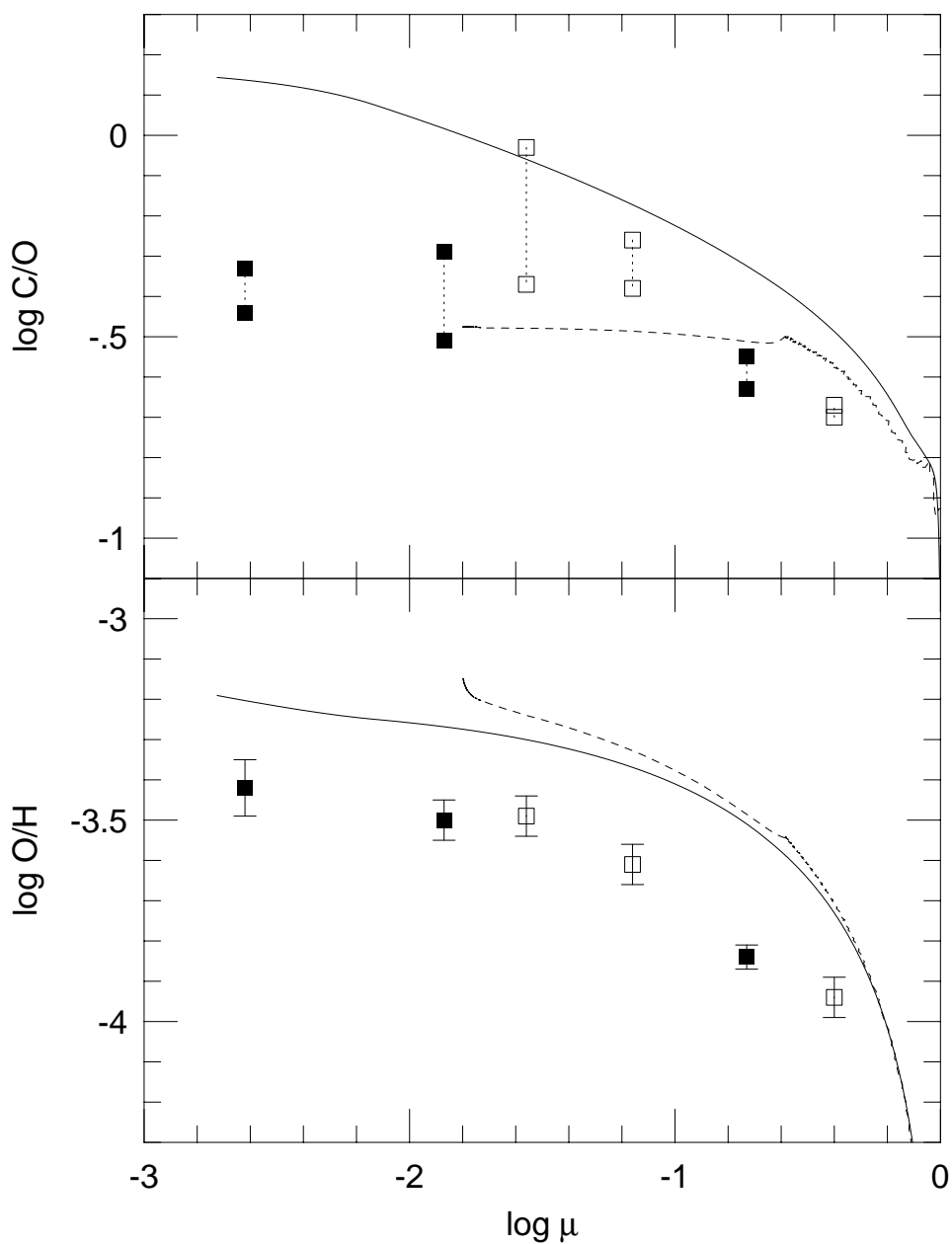


Fig. 7.— Abundance ratios for the NGC 2403 and M101 regions plotted against the natural logarithm of the gas fraction. Dashed lines connect values for the same regions, but computed with different reddening laws. Open symbols are the M101 regions, filled symbols the NGC 2403 regions. The solid lines show the predictions for the “best” model from Carigi (1996); the dashed line is the model of Chiappini et al. (1997).

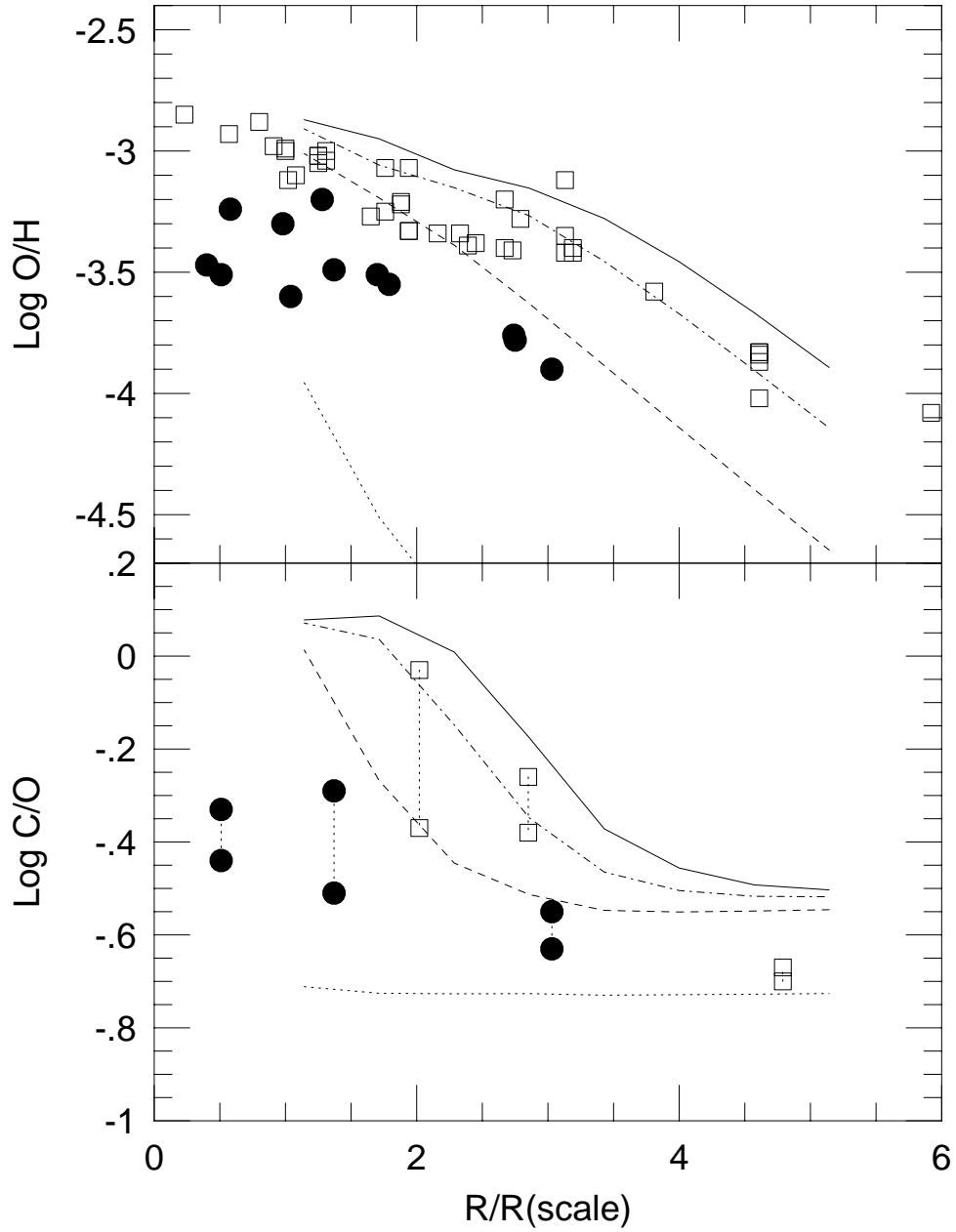


Fig. 8.— C and O abundances in NGC 2403 and M101 plotted as a function of galactocentric radius normalized by the disk scale length. Open symbols: M101; filled symbols: NGC 2403. The top panel includes all the O/H measurements from Kennicutt & Garnett (1996) and Garnett et al. (1997b). The lines show model results for the Milky Way from Carigi (1996) for four different ages: dotted line = 0.5 Gyr; dashed = 4 Gyr; dot-dash = 9 Gyr; solid = 13 Gyr.

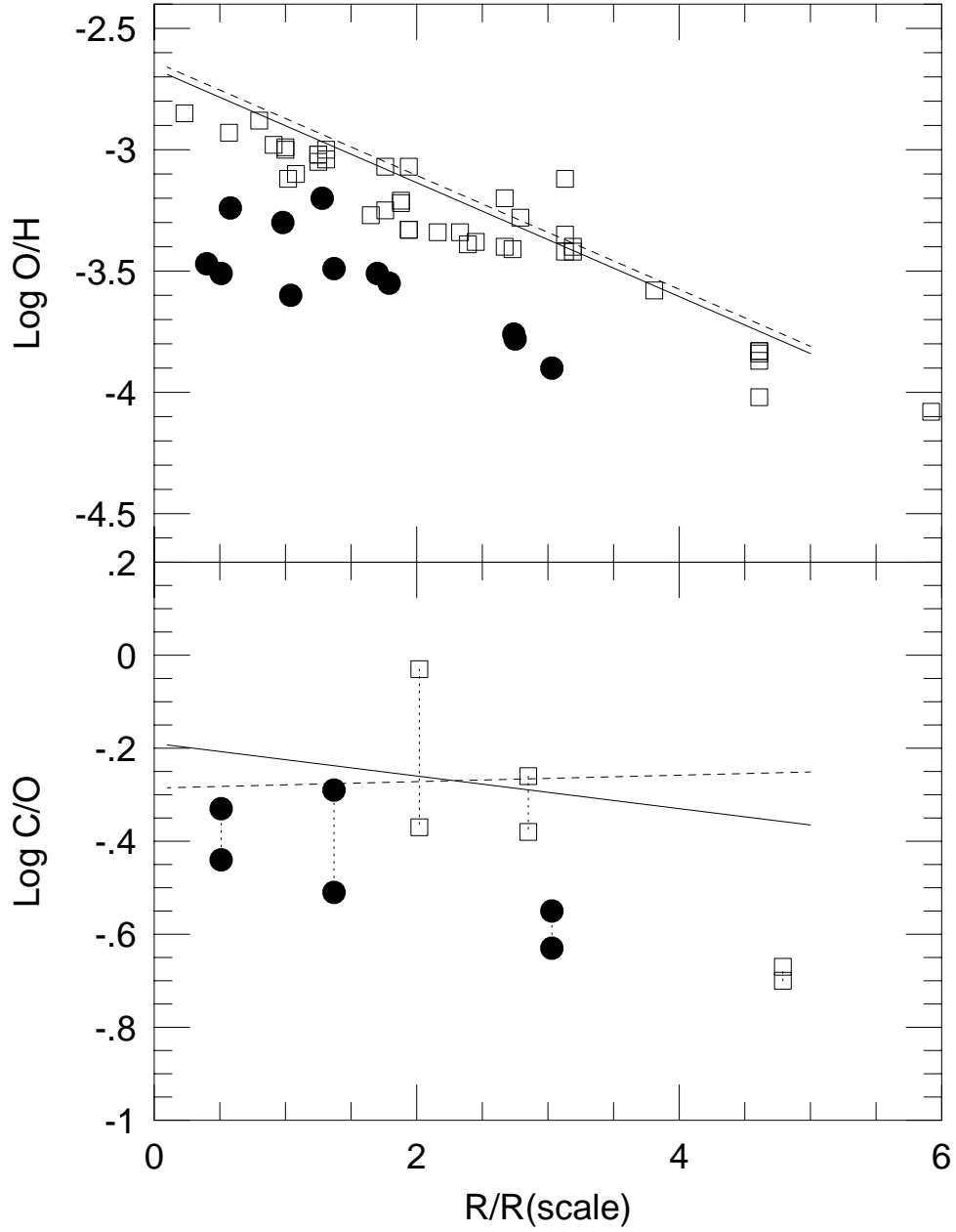


Fig. 9.— Same as Figure 8, but showing Milky Way model calculations from Götzt & Köppen (1992) and Mollá et al. (1997). Solid line: Mollá et al.; dashed: Götzt & Köppen.

Table 1. Journal of HST Observations

Observation ID	Date	Target	RA (J2000)	DEC (J2000)	Disperser	Exp. Time
Y30A0402T	11 Apr 1996	M101-NGC5471	14:04:29.02	+54:23:48.8	G190H	1500s
Y30A0404T	11 Apr 1996	M101-NGC5471			G190H	1260s
Y30A0406T	11 Apr 1996	M101-NGC5471			G400H	390s
Y30A0408T	11 Apr 1996	M101-NGC5471			G570H	40s
Y30A0409M	11 Apr 1996	M101-NGC5471			G570H	340s
Y30A040AM	11 Apr 1996	M101-NGC5471			G270H	1200s
Y30A0502T	12 Apr 1996	M101-NGC5461	14:03:41.62	+54:19:04.4	G190H	1500s
Y30A0504T	12 Apr 1996	M101-NGC5461			G190H	1260s
Y30A0506T	12 Apr 1996	M101-NGC5461			G400H	390s
Y30A0508T	12 Apr 1996	M101-NGC5461			G570H	40s
Y30A0509T	12 Apr 1996	M101-NGC5461			G570H	310s
Y30A050AT	12 Apr 1996	M101-NGC5461			G270H	1200s
Y30A0602T	04 Apr 1996	M101-NGC5455	14:03:01.16	+54:14:27.0	G190H	1680s
Y30A0604T	04 Apr 1996	M101-NGC5455			G190H	2580s
Y30A0606T	04 Apr 1996	M101-NGC5455			G400H	600s
Y30A0608T	04 Apr 1996	M101-NGC5455			G270H	1500s
Y30A060AT	04 Apr 1996	M101-NGC5455			G270H	1080s
Y30A060CT	04 Apr 1996	M101-NGC5455			G570H	300s
Y30A0102T	13 Nov 1995	NGC2403-VS9	07:36:28.63	+65:33:49.0	G270H	2430s
Y30A0104T	13 Nov 1995	NGC2403-VS9			G190H	3600s
Y30A0106T	13 Nov 1995	NGC2403-VS9			G400H	360s
Y30A0108T	13 Nov 1995	NGC2403-VS9			G570H	360s
Y30A0302T	25 Feb 1996	NGC2403-VS38	07:36:52.13	+65:36:48.5	G190H	3540s
Y30A0304T	25 Feb 1996	NGC2403-VS38			G190H	3540s
Y30A0306T	25 Feb 1996	NGC2403-VS38			G570H	330s
Y30A0308T	25 Feb 1996	NGC2403-VS38			G400H	390s
Y30A0309T	25 Feb 1996	NGC2403-VS38			G270H	3840s
Y30A5202T	29 Jan 1997	NGC2403-VS44	07:37:06.82	+65:36:38.7	G190H	3460s
Y30A5204T	29 Jan 1997	NGC2403-VS44			G270H	2560s
Y30A5206T	29 Jan 1997	NGC2403-VS44			G400H	390s

Table 1—Continued

Observation ID	Date	Target	RA (J2000)	DEC (J2000)	Disperser	Exp. Time
Y30A5208T	29 Jan 1997	NGC2403-VS44			G570H	300s

Table 2. FOS Spectra for M101 and NGC 2403 H II Regions

Line ID	$I_{\lambda}(obs)/I(H\beta)$	$I_{\lambda}(corr)/I(H\beta)$ $R_V = 3.1$	$I_{\lambda}(corr)/I(H\beta)$ $R_V = 5$
NGC 5455			
O III] 1666	< 0.13	< 0.25	< 0.17
N III] 1750	< 0.13	< 0.24	< 0.17
Si III] 1883	< 0.10	< 0.20	< 0.14
C III] 1909	0.14 (0.05)	0.27 (0.11)	0.20 (0.07)
N II] 2140	< 0.05	< 0.13	< 0.09
C II] 2325	0.10 (0.03)	0.21 (0.07)	0.16 (0.05)
[O II] 2470	< 0.03	< 0.05	< 0.04
He I 2945	< 0.02	< 0.03	< 0.02
He I 3188	< 0.02	< 0.03	< 0.02
[O II] 3727	2.65 (0.09)	3.14 (0.16)	3.05 (0.14)
H 10 3795	< 0.06	< 0.07	< 0.07
H 9 3835	< 0.06	< 0.07	< 0.07
[Ne III] 3869	0.16 (0.03)	0.19 (0.04)	0.18 (0.03)
H δ 4102	0.20 (0.03)	0.27 (0.04)	0.27 (0.04)
H γ 4340	0.40 (0.03)	0.47 (0.04)	0.46 (0.04)
[O III] 4363	< 0.06	< 0.07	< 0.06
He I 4471	< 0.06	< 0.06	< 0.06
H β 4861	1.00 (0.05)	1.00 (0.05)	1.00 (0.05)
[O III] 4959	0.95 (0.06)	0.94 (0.06)	0.94 (0.06)
[O III] 5007	2.93 (0.10)	2.87 (0.10)	2.85 (0.10)
He I 5876	< 0.10	< 0.09	< 0.09
H α 6563	3.47 (0.11)	2.88 (0.14)	2.85 (0.14)
[N II] 6584	0.52 (0.05)	0.44 (0.05)	0.44 (0.05)
[S II] 6725	0.65 (0.08)	0.55 (0.07)	0.54 (0.07)
A(H β) (mag.)		0.58 (0.13)	0.80 (0.17)

Table 2—Continued

Line ID	$I_{\lambda}(obs)/I(H\beta)$	$I_{\lambda}(corr)/I(H\beta)$ $R_V = 3.1$	$I_{\lambda}(corr)/I(H\beta)$ $R_V = 5$
NGC 5461			
[O III] 1666	< 0.12	< 0.54	< 0.22
N III] 1750	< 0.05	< 0.22	< 0.09
Si III] 1883	< 0.03	< 0.15	< 0.07
C III] 1909	0.06 (0.02)	0.30 (0.11)	0.13 (0.04)
N II] 2140	< 0.02	< 0.19	< 0.08
C II] 2325	0.06 (0.02)	0.35 (0.12)	0.18 (0.06)
[O II] 2470	0.08 (0.01)	0.30 (0.05)	0.17 (0.02)
He I 2945	< 0.02	< 0.04	< 0.03
He I 3188	< 0.02	< 0.04	< 0.03
[O II] 3727	2.05 (0.06)	3.09 (0.12)	2.86 (0.10)
H 10 3795	0.08 (0.02)	0.12 (0.03)	0.11 (0.03)
H 9 3835	0.07 (0.02)	0.10 (0.03)	0.10 (0.03)
[Ne III] 3869	0.12 (0.02)	0.17 (0.03)	0.16 (0.03)
H δ 4102	0.22 (0.02)	0.30 (0.03)	0.28 (0.03)
H γ 4340	0.40 (0.02)	0.49 (0.03)	0.48 (0.03)
[O III] 4363	< 0.03	< 0.04	< 0.04
He I 4471	< 0.03	< 0.04	< 0.03
H β 4861	1.00 (0.03)	1.00 (0.03)	1.00 (0.03)
[O III] 4959	0.98 (0.03)	0.95 (0.03)	0.95 (0.03)
[O III] 5007	3.25 (0.10)	3.10 (0.10)	3.12 (0.10)
He I 5876	0.12 (0.02)	0.09 (0.02)	0.09 (0.02)
H α 6563	4.44 (0.14)	3.03 (0.12)	2.96 (0.12)
[N II] 6584	0.63 (0.03)	0.43 (0.02)	0.42 (0.02)
[S II] 6725	0.71 (0.04)	0.47 (0.03)	0.46 (0.03)
A(H β) (mag.)		1.39 (0.09)	1.91 (0.12)

Table 2—Continued

Line ID	$I_{\lambda}(obs)/I(H\beta)$	$I_{\lambda}(corr)/I(H\beta)$ $R_V = 3.1$	$I_{\lambda}(corr)/I(H\beta)$ $R_V = 5$
NGC 5471			
[O III] 1666	< 0.28	< 0.30	< 0.28
N III] 1750	< 0.16	< 0.17	< 0.16
Si III] 1883	0.17 (0.08)	0.18 (0.09)	0.17 (0.08)
C III] 1909	0.47 (0.06)	0.50 (0.08)	0.48 (0.07)
N II] 2140	< 0.06	< 0.07	< 0.06
C II] 2325	< 0.07	< 0.08	< 0.07
[O II] 2470	< 0.05	< 0.05	< 0.05
He I 2945	< 0.04	< 0.04	< 0.04
He I 3188	< 0.03	< 0.03	< 0.03
[O II] 3727	1.74 (0.06)	1.77 (0.07)	1.76 (0.07)
H 10 3795	< 0.04	< 0.04	< 0.04
H 9 3835	0.05 (0.02)	0.05 (0.02)	0.05 (0.02)
[Ne III] 3869	0.50 (0.02)	0.51 (0.02)	0.50 (0.02)
H δ 4102	0.27 (0.02)	0.27 (0.02)	0.27 (0.02)
H γ 4340	0.48 (0.02)	0.48 (0.02)	0.48 (0.02)
[O III] 4363	0.08 (0.02)	0.08 (0.02)	0.08 (0.02)
He I 4471	< 0.04	< 0.04	< 0.04
H β 4861	1.00 (0.04)	1.00 (0.04)	1.00 (0.04)
[O III] 4959	1.96 (0.06)	1.96 (0.06)	1.96 (0.06)
[O III] 5007	5.44 (0.16)	5.43 (0.16)	5.43 (0.16)
He I 5876	0.14 (0.03)	0.14 (0.03)	0.14 (0.03)
H α 6563	2.92 (0.10)	2.88 (0.12)	2.88 (0.12)
[N II] 6584	0.14 (0.04)	0.14 (0.04)	0.14 (0.04)
[S II] 6725	< 0.13	< 0.13	< 0.13
A(H β) (mag.)		0.05 (0.08)	0.06 (0.12)

Table 2—Continued

Line ID	$I_{\lambda}(obs)/I(H\beta)$	$I_{\lambda}(corr)/I(H\beta)$ $R_V = 3.1$	$I_{\lambda}(corr)/I(H\beta)$ $R_V = 5$
VS 38			
O III] 1666	< 0.04	< 0.1	< 0.06
N III] 1750	< 0.02	< 0.05	< 0.03
Si III] 1883	< 0.016	< 0.04	< 0.03
C III] 1909	< 0.017	< 0.05	< 0.03
N II] 2140	< 0.008	< 0.03	< 0.02
C II] 2325	0.035 (0.008)	0.10 (0.03)	0.07 (0.02)
[O II] 2470	< 0.012 (0.005)	0.03 (0.01)	0.019 (0.008)
He I 2945	< 0.009	< 0.02	< 0.01
He I 3188	< 0.028 (0.004)	0.040 (0.006)	0.035 (0.005)
[O II] 3727	1.726 (0.053)	2.2 (0.1)	2.10 (0.09)
H 10 3795	0.033 (0.009)	0.04 (0.01)	0.04 (0.01)
H 9 3835	0.045 (0.009)	0.06 (0.01)	0.05 (0.01)
[Ne III] 3869	0.073 (0.009)	0.09 (0.01)	0.09 (0.01)
H δ 4102	0.246 (0.014)	0.29 (0.02)	0.28 (0.02)
H γ 4340	0.448 (0.016)	0.51 (0.02)	0.50 (0.02)
[O III] 4363	< 0.018	< 0.02	< 0.02
He I 4471	0.044 (0.009)	0.05 (0.01)	0.05 (0.01)
H β 4861	1.000 (0.032)	1.00 (0.03)	1.00 (0.03)
[O III] 4959	0.553 (0.021)	0.54 (0.02)	0.54 (0.02)
[O III] 5007	1.833 (0.057)	1.78 (0.06)	1.80 (0.06)
He I 5876	0.175 (0.012)	0.15 (0.01)	0.15 (0.01)
[S III] 6312	< 0.033	< 0.03	< 0.03
H α 6563	3.927 (0.118)	3.1 (0.1)	3.1 (0.1)
[N II] 6584	0.494 (0.022)	0.39 (0.02)	0.39 (0.02)
[S II] 6725	0.202 (0.041)	0.16 (0.03)	0.16 (0.03)
A(H β)		0.8 (0.1)	1.0 (0.2)

Table 2—Continued

Line ID	$I_{\lambda}(obs)/I(H\beta)$	$I_{\lambda}(corr)/I(H\beta)$ $R_V = 3.1$	$I_{\lambda}(corr)/I(H\beta)$ $R_V = 5$
VS 44			
O III] 1666	0.017 (0.014)	0.04 (0.03)	0.02 (0.02)
N III] 1750	< 0.016	< 0.04	< 0.03
Si III] 1883	< 0.015	< 0.04	< 0.03
C III] 1909	0.057 (0.007)	0.15 (0.03)	0.09 (0.01)
N II] 2140	< 0.007	< 0.03	< 0.02
C II] 2325	0.039 (0.004)	0.11 (0.02)	0.071 (0.009)
[O II] 2470	0.029 (0.004)	0.06 (0.01)	0.045 (0.007)
He I 2945	0.008 (0.002)	0.013 (0.003)	0.010 (0.003)
He I 3188	0.022 (0.003)	0.031 (0.004)	0.027 (0.004)
[O II] 3727	1.803 (0.054)	2.3 (0.1)	2.17 (0.08)
H 12 3750	0.015 (0.006)	0.019 (0.008)	0.018 (0.007)
H 11 3770	0.017 (0.006)	0.021 (0.008)	0.020 (0.007)
H 10 3795	0.024 (0.006)	0.030 (0.008)	0.029 (0.007)
H 9 3835	0.042 (0.005)	0.053 (0.006)	0.050 (0.006)
[Ne III] 3869	0.125 (0.006)	0.16 (0.01)	0.15 (0.01)
He I 4026	0.024 (0.005)	0.029 (0.006)	0.028 (0.006)
H δ 4102	0.251 (0.008)	0.30 (0.01)	0.29 (0.01)
H γ 4340	0.440 (0.013)	0.50 (0.02)	0.48 (0.02)
[O III] 4363	< 0.009	< 0.01	< 0.01
He I 4471	0.031 (0.005)	0.034 (0.006)	0.033 (0.005)
H β 4861	1.000 (0.030)	1.00 (0.03)	1.00 (0.03)
[O III] 4959	0.964 (0.030)	0.94 (0.03)	0.95 (0.03)
[O III] 5007	2.922 (0.088)	2.86 (0.09)	2.87 (0.09)
He I 5876	0.141 (0.007)	0.12 (0.01)	0.12 (0.01)
[S III] 6312	0.017 (0.005)	0.014 (0.004)	0.014 (0.004)
H α 6563	3.787 (0.114)	3.0 (0.1)	3.1 (0.1)
[N II] 6584	0.459 (0.016)	0.37 (0.02)	0.37 (0.02)
He I 6678	0.053 (0.007)	0.042 (0.006)	0.043 (0.006)
[S II] 6717	0.127 (0.008)	0.10 (0.01)	0.10 (0.01)
[S II] 6731	0.127 (0.008)	0.10 (0.01)	0.10 (0.01)
A(H β)		0.7 (0.1)	0.9 (0.1)

Table 2—Continued

Line ID	$I_\lambda(obs)/I(H\beta)$	$I_\lambda(corr)/I(H\beta)$ $R_V = 3.1$	$I_\lambda(corr)/I(H\beta)$ $R_V = 5$
---------	----------------------------	--	--

Table 2—Continued

Line ID	$I_{\lambda}(obs)/I(H\beta)$	$I_{\lambda}(corr)/I(H\beta)$ $R_V = 3.1$	$I_{\lambda}(corr)/I(H\beta)$ $R_V = 5$
VS 9			
O III] 1666	< 0.38	< 0.5	< 0.4
N III] 1750	< 0.27	< 0.4	< 0.3
Si III] 1883	< 0.17	< 0.2	< 0.2
C III] 1909	0.363 (0.082)	0.4 (0.2)	0.3 (0.1)
N II] 2140	< 0.10	< 0.2	< 0.1
C II] 2325	0.102 (0.052)	0.14 (0.08)	0.12 (0.06)
[O II] 2470	< 0.10	< 0.1	< 0.1
He I 2945	< 0.06	< 0.07	< 0.07
He I 3188	< 0.06	< 0.07	< 0.07
[O II] 3727	2.004 (0.085)	2.2 (0.2)	2.1 (0.1)
H 10 3795	< 0.15	< 0.2	< 0.2
H 9 3835	< 0.15	< 0.2	< 0.2
[Ne III] 3869	0.288 (0.062)	0.31 (0.07)	0.30 (0.07)
H δ 4102	< 0.26	< 0.3	< 0.3
H γ 4340	0.465 (0.064)	0.48 (0.07)	0.48 (0.07)
[O III] 4363	< 0.12	< 0.1	< 0.1
He I 4471	< 0.13	< 0.1	< 0.1
H β 4861	1.000 (0.068)	1.00 (0.07)	1.00 (0.07)
[O III] 4959	1.225 (0.069)	1.22 (0.07)	1.22 (0.07)
[O III] 5007	4.092 (0.137)	4.0 (0.1)	4.0 (0.1)
He I 5876	< 0.10	< 0.1	< 0.1
[S III] 6312	< 0.11	< 0.1	< 0.1
H α 6563	3.125 (0.111)	2.9 (0.2)	2.9 (0.2)
[N II] 6584	0.393 (0.062)	0.37 (0.06)	0.37 (0.06)
[S II] 6725	< 0.22	< 0.2	< 0.2
A(H β)		0.2 (0.2)	0.3 (0.3)

Table 3. Adopted Electron Densities and Electron Temperatures

Object	n_e (cm^{-3})	T[O III] (K)	T[O II] (K)
NGC 5455	100	9700±500	9800±600
NGC 5461	100	9000±300	9300±500
NGC 5471	100	13200±300	12200±500
VS 38	100	7600±600	8300±600
VS 44	600	8700±400	9100±600
VS 9	100	11700±400	11200±400

Table 4. Ionic Abundances from FOS Observations

Object	$\log \frac{O^+}{H^+}$	$\log \frac{O^{+2}}{H^+}$	$\log \frac{C^+}{H^+}$ $R_V = 3.1$	$\log \frac{C^+}{H^+}$ $R_V = 5$	$\log \frac{C^{+2}}{H^+}$ $R_V = 3.1$	$\log \frac{C^{+2}}{H^+}$ $R_V = 5$
NGC 5455	-3.89 ± 0.07	-3.93 ± 0.05	-4.32 ± 0.14	-4.44 ± 0.14	-4.05 ± 0.16	-4.18 ± 0.15
NGC 5461	-3.79 ± 0.05	-3.78 ± 0.03	-3.93 ± 0.14	-4.22 ± 0.14	-3.73 ± 0.15	-4.10 ± 0.13
NGC 5471	-4.55 ± 0.04	-4.06 ± 0.03	< -5.3	< -5.4	-4.70 ± 0.07	-4.72 ± 0.07
VS 38	-3.69 ± 0.07	-3.76 ± 0.07	-4.12 ± 0.15	-4.30 ± 0.15	-4.00 ± 0.16	-4.16 ± 0.16
VS 44	-3.83 ± 0.06	-3.78 ± 0.04	-4.38 ± 0.11	-4.57 ± 0.10	-3.92 ± 0.11	-4.15 ± 0.09
VS 9	-4.28 ± 0.05	-4.04 ± 0.04	-4.85 ± 0.20	-4.92 ± 0.18	-4.57 ± 0.18	-4.66 ± 0.13

Table 5. Total Abundances for NGC 2403 and M101 H II Regions

Object	log O/H	log C/O $R_V = 3.1$	log C/O $R_V = 5$	log N/O
NGC 5455	-3.61 ± 0.03	-0.26 ± 0.14	-0.38 ± 0.13	-1.18 ± 0.10
NGC 5461	-3.49 ± 0.03	-0.03 ± 0.13	-0.37 ± 0.12	-1.13 ± 0.06
NGC 5471	-3.94 ± 0.03	-0.67 ± 0.05	-0.70 ± 0.05	-1.33 ± 0.06
VS 38	-3.42 ± 0.05	-0.33 ± 0.12	-0.44 ± 0.11	-1.08 ± 0.03
VS 44	-3.50 ± 0.04	-0.29 ± 0.08	-0.51 ± 0.07	-1.19 ± 0.03
VS 9	-3.84 ± 0.03	-0.55 ± 0.19	-0.63 ± 0.15	-1.21 ± 0.03